This is a post-refereeing final draft. When citing, please refer to the published version:

S. Cruz-Manzo, P. Greenwood and R. Chen, J. Electrochem. Soc. 2017 volume 164, issue 7, A1446-A1453.

An Impedance Model for EIS Analysis of Nickel Metal Hydride Batteries

Samuel Cruz-Manzo[1*], Paul Greenwood[2], Rui Chen[3]

[1]School of Engineering, University of Lincoln, Lincolnshire, LN6 7TS, United Kingdom

[2]Abastecedora Electrica Tehuacan, Engineering Division, Tehuacan, Puebla, 75700, Mexico

[3]Department of Aeronautical and Automotive Engineering, Loughborough University, Leicestershire, LE11 3TU, United Kingdom

[*]s.cruz-manzo@hotmail.com

Abstract

Based on fundamental electrochemical theory, an impedance model for analysis of electrochemical impedance spectroscopy (EIS) of Nickel-Metal Hydride (NiMH) batteries is presented in this study. The resulting analytical expression is analogous to the impedance response of the Randles electrical circuit used for EIS analysis on NiMH batteries. The impedance model is validated against EIS measurements carried out whilst decreasing the state of charge (SOC) of a NiMH battery pack. The diffusion mechanisms during the discharge of the NiMH battery is modelled through a Warburg element derived from diffusion theory considering reflective boundary conditions. ZView® Scribner Associates Inc. software allowed the estimation of electrochemical and diffusion parameters from EIS measurements of the NiMH battery. The effect of diffusion mechanisms on EIS measurements is discussed. The results demonstrate that ion transport is the rate-limiting process during the discharge of the NiMH battery. This EIS-modelling study has provided an insight into the interpretation of battery electrochemical mechanisms represented in the Nyquist plot from EIS. It can assist to further EIS-modelling to study and correlate State of Health (SOH) in NiMH batteries for different applications.

1. Introduction

The Nickel-Metal Hydride (NiMH) battery is known to be as an alkaline storage battery due to its electrolyte based on potassium hydroxide KOH. NiMH batteries have many applications from portable consumer products to Hybrid Electric Vehicles (HEVs). HEVs are touted as providing a long-term solution to reduce automotive CO_2 emissions. The high battery costs limit the HEV development and marketing. It is desirable to replace the battery when the performance drops below 80% of their initial capacity to maintain the resale value for low demand stationary applications. However, the service life of the battery stack in HEV applications is unpredictable as it is continuously recharged and is sensitive to the environment. It needs to be regularly tested [1]. The most common performance test for batteries consists of the discharge of the battery through a load bank and the measurement of the amount of stored energy. This procedure may be destructive to the battery, if improperly performed. Other available testing procedures [2,3,4] are useful for identifying batteries in extremely poor conditions.

Electrochemical impedance spectroscopy (EIS) is an experimental technique that allows the characterisation of physical processes of electrochemical systems. Many studies have applied EIS to batteries because the change of the battery EIS response can be an asset to evaluate the state of charge (SOC) for different charge-discharge cycles [5,6,7]. The change in the EIS response in batteries has been related to changes in electrode porosity, electrode sulphatation, and electrolyte concentration [5]. Some studies have attempted the estimation of the SOC in batteries (NiMH, Lead-Acid, lithium-ion, lithium-iron phosphate) through EIS measurements and equivalent electrical circuits [8,9,10,11,12,13,14,15]. Different configurations for circuits have been applied in EIS measurements but without a full understanding of the electrochemical mechanisms of the battery represented in the Nyquist plot obtained from EIS. The Randles circuit for NiMH battery analysis [13,14,15] consists of an active electrolyte resistance in series with a parallel combination of the double-layer capacitance in the electrode and a resistor of a Faradaic reaction, as shown in Fig. 1. A constant phase element (CPE) is commonly used instead of a pure capacitor to correct for the inhomogeneity distribution of charge in the electrode [14,16]. A Warburg element Z_W [17] representing the diffusion process is connected in series with the resistor R_C of the Faradaic reaction, as shown in Fig.1. The infinite-length Warburg component is commonly used and considers diffusion of a particle in semi-infinite space [18]. Some studies [19,20,21] have opted to connect the Warburg element in series with the resistor-capacitor parallel configuration. In this configuration, the impedance of the Warburg element is independent from the impedance of

the parallel combination of the double-layer capacitance and a resistor of a Faradaic reaction. Buller *et al.* [20] reported that this configuration does not lead to significant deviation in the simulation results, but an analytical derivation of this configuration from electrochemical theory was not provided. Scholz [18] derived the impedance response of the Randles circuit shown in Fig. 1 considering the Warburg element Z_W from a semi-infinite linear diffusion of charged particles in the electrode. Song and Bazant [22] reported the effects of nanoparticle geometry and size distribution on diffusion impedance of battery electrodes. The authors reported that the impedance spectra of modern thin film and nanoparticle battery electrodes show a distinguished feature in the diffusion impedance: the response transitions from the original Warburg behaviour to a capacitive behaviour at a lower frequency range. The authors also reported that the Warburg-Capacitive behaviour was attributed to bounded diffusion space in active material due to the short diffusion lengths in the thin film in the electrode where the diffusion penetration depth can reach the reflective center of a nanoparticle at accessible low frequencies.

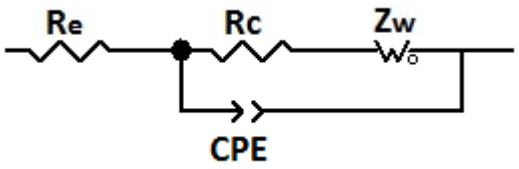

Figure 1. Electrical circuit for analysis of NiMH batteries through EIS

A standard mathematical algorithm based on a process model is needed to lead the EIS-based studies of the battery towards physical and electrochemical interpretation of battery processes. Taking into consideration this, the biggest challenge is that the interpretation of the electrochemical mechanisms which are truly occurring in the battery using EIS will only be possible through a new but robust mathematical algorithm which is derived from fundamental electrochemical theory. Also, the correct interpretation of the electrochemical mechanisms causing a change in EIS response in batteries at different charge and discharge cycles can only be achieved through mathematical models or electrical circuits derived from fundamental electrochemical theory. The objective of this study is to provide an insight into the electrochemical mechanisms, represented in the Nyquist plot from EIS, during the discharge of a NiMH battery. The resulting mathematical treatment could assist further EIS modelling to study other mechanisms in NiMH batteries which can be manifested at abnormal severe operating conditions.

2. NiMH Battery Electrochemistry

The positive electrode (cathode) of a NiMH battery is composed of nickel hydroxide, and the negative electrode (anode) is composed of a metal hydride *MH* structure where hydrogen ions are stored. The electrolyte between both electrodes is composed of an alkaline substance (potassium hydroxide *KOH*) [23]. The overall NiMH battery reaction is expressed as [24]:

$$MH + NiOOH \underset{charge}{\overset{discharge}{\rightleftharpoons}} M + Ni(OH)_2 \quad (1)$$

During the discharging process the metal hydride *MH* in the anode and hydroxide ions OH^- from the electrolyte react to produce water and one free electron e^-. In the cathode, nickel oxyhydroxide $NiOOH$ combines with water from the electrolyte and the one free electron to produce nickel hydroxide $Ni(OH)_2$. When the battery is charged, reverse electrochemical reactions take place at both electrodes. The following assumptions have been considered for the development of the theoretical model:

- The mathematical treatment and experimental validation considers only the electrochemical mechanisms during the discharge of a NiMH battery.

- Only the electrochemical reaction and diffusive processes during the reaction $NiOOH + H_2O + e^- \rightarrow Ni(OH)_2 + OH^-$ at the cathode or positive electrode is considered.

- No intermediate electrochemical process for reaction 1 are considered.

- No overdischarge reaction at abnormal severe operating conditions [24] is considered. This will be studied in future work to predict SOH through EIS-modelling.

- No transformation of the $NiOOH$ occurs in the KOH solution [25].

- As EIS measurements are carried out at open circuit condition, reflective boundary conditions [18] are considered in the mathematical treatment related to diffusion.

The electrochemical reactions at the positive electrode of the NiMH battery can be represented through an electron-transfer reaction [26].

$$Ox + e^{-} \rightarrow \mathrm{Re} \tag{2}$$

where *Ox* is the oxidized form of the reactant and *Re* is the reduced form of the reactant, and e^{-} the electrons transferred. Zimmerman and Effa [27] and Zhu *et al.* [14] reported that water taking part in the reduction process of $NiOOH + H_2O + e^{-} \rightarrow Ni(OH)_2 + OH^{-}$ can be disassociated as follows: water transport from bulk electrolyte to the electrode/electrolyte interface, formation of a proton and hydroxide ion at catalytic site at interface, and diffusion of the proton from the surface site to the charge transfer site in the electrode bulk.

The Butler-Volmer Equation describes the non-linear relation between current and overpotential [28] as such:

$$i_F = \vartheta_O i_0 \exp(-\alpha f \eta) - \vartheta_R i_0 \exp((1-\alpha) f \eta) \tag{3}$$

with $\eta = V - E^0$, $\vartheta_{O,R} = c_{O,R} / c^*_{O,R}$, and $f = zF / RT$, where η is the overpotential, E^0 is the potential at equilibrium conditions, V is the battery voltage, $c_{O,R}$ is the concentration of oxidized (protons [29]) and reduced (nickel hydroxide [30]) chemical species at the electrode surface, $c^*_{O,R}$ is the bulk concentration of oxidized and reduced chemical species, ϑ is the ratio between chemical species at the electrode surface and bulk concentration of chemical species, i_0 is the exchange current, F is the Faraday constant, R is the gas constant, T is the temperature, α is the exchange transfer coefficient, and i_F is the Faradaic current. Eq. 3 considers that the concentration of oxidized and reduced chemical species at the electrode surface is different from the bulk concentration $\vartheta_{O,R} < 1$. Some studies [31,32] have considered the assumption $\vartheta_{O,R} \approx 1$ in Eq. 3 to simplify battery modelling; however, this assumption is only valid at low battery current.

When the overpotential η becomes more negative according to $\eta = V - E^0$ during the discharging process, the contribution of the second term on the right-hand side of Eq. 3 becomes small, and therefore it can be neglected. The value of the second term in Eq. 3 can be neglected for $|\eta| > 0.1V$ considering $\vartheta_R = 1, \alpha = 0.5$ $i_0 = 0.1 mA/cm^2$ [30].

$$i_F = \vartheta_O i_0 \exp(-\eta / b) \tag{4}$$

where $b = RT / zF\alpha$ is the Tafel slope.

If a small ac perturbation is applied to the working electrode, the EIS technique allows the use of a linear equation to simulate impedance spectra. A linear model can be derived using the Taylor series expansion as expressed below:

$$\tilde{i} = \left(\frac{\partial i}{\partial V}\right)_{ss} \tilde{V} + \left(\frac{\partial i}{\partial \vartheta}\right)_{ss} \tilde{\vartheta} \tag{5}$$

Applying Eq. 5 to Eq. 4 yields:

$$\tilde{i_F} = -\frac{\vartheta_{ss} i_0 \exp(-\eta_{ss} / b)}{b} \tilde{V} + i_0 \exp(-\eta_{ss} / b) \tilde{\vartheta} \tag{6}$$

Where $\eta_{SS} = V_{SS} - E^0$ represent the overpotential at steady state and ϑ_{ss} is the ratio of concentration of chemical species at steady state.

Eq. 6 can be expressed as:

$$\tilde{i_F} = \frac{1}{R_C} \tilde{V} + i_0 \exp(-\eta_{ss} / b) \tilde{\vartheta} \tag{7}$$

with

$$R_C = -\frac{b}{\vartheta_{ss} i_0 \exp(-\eta_{ss} / b)} \tag{8}$$

which represents the charge transfer resistance during the chemical reaction at the positive electrode.

2.1 Diffusion Theory

Fick's Second Law is considered to model the effect of diffusion on the distribution of concentration of chemical species with respect to time, as such:

$$D\frac{\partial^2 c_O(x,t)}{\partial x^2} = \frac{\partial c_O(x,t)}{\partial t} \tag{9}$$

EIS measurements are carried out at steady state. At steady state the concentration of chemical species is independent of time; hence Fick's Second Law can be expressed in Laplace domain *s*. D is the effective diffusion coefficient. The solution of Eq. 9 in the Laplace domain requires an initial condition in *t*=0 as $c_O(x,0)=0$. This solution in the Laplace domain through the method of *nth-order homogeneous equations with constant coefficients* (see Appendix A) takes the form of:

$$c_O(x,s) = A\exp(\lambda_1 x) + B\exp(\lambda_2 x) \tag{10}$$

where $\lambda_{1,2} = \pm\sqrt{s/D}$ represents the distinct roots of the characteristic equation, *x* is the distance for chemical species to diffuse in the electrode from *x=0* up to a diffusion distance *x=δ*. Song and Bazant [22] developed theoretical diffusion impedance models to study effects of nanoparticle geometry and size distribution on battery electrodes. The impedance diffusion models considered reflective boundary conditions [33]. A pseudo-vertical line at low frequencies in the Nyquist plot of EIS in NiMH batteries is commonly represented [13,15]. Scholz [18] reported that a pseudo-vertical line at low frequencies is attributed to a complete blocking diffusion during open circuit conditions which can be defined as diffusion with reflective boundary conditions. In this study, the EIS measurements in the NiMH battery are carried out at open circuit (steady-state) to comply with stability conditions of Kramers-Kronig [34]. This will be discussed in the experimental and validation section. Therefore, the diffusion of the chemical species in the NiMH battery will be considered with reflective boundary conditions.

Considering a boundary condition in Eq. 10 as:

$$\left.\frac{dc_O}{dx}\right|_{x=0} = 0 \tag{11}$$

To comply with the boundary condition Eq. 11, therefore Eq. 10 can be expressed as:

$$c_O(x,s) = A\left[\exp(\lambda_1 x) + \exp(-\lambda_1 x)\right] \tag{12}$$

where the value of A will depend on a second boundary condition which is defined from Fick's First Law.

From Faraday's Law, it is possible to establish that the current density in the Laplace domain is proportional to the charge transferred and the consumption of reactant:

$$i_F(s) = zFv(s) \tag{13}$$

where $v(s)$ is the flux of reactant, and F is the Faraday constant.

From Fick's First Law it is possible to establish that the flux of reactant is proportional to concentration gradient

$$v(s) = -D\left.\frac{dc_O(x,s)}{dx}\right|_{x=\delta} \tag{14}$$

where D is the effective diffusion coefficient of chemical species and x is the distance for the chemical species to diffuse.

In steady state the current from Faraday's Law is equal to the diffusion flux from Fick's First Law. Combining Eqs. 13, and 14 yields:

$$\frac{i_F(s)}{zF} = -D\left.\frac{dc_O(x,s)}{dx}\right|_{x=\delta} \tag{15}$$

Differentiating Eq. 12 with respect to the distance x yields:

$$\frac{dc_O(x,s)}{dx} = \lambda_1 A\left[\exp(\lambda_1 x) - \exp(-\lambda_1 x)\right] \tag{16}$$

Substituting Eq. 16 into Eq. 15 with $x=\delta$ yields:

$$A = -\frac{i_F(s)}{zFD\lambda_1\left[\exp(\lambda_1\delta) - \exp(-\lambda_1\delta)\right]} \tag{17}$$

Substituting Eq. 17 into Eq. 12 yields:

$$c_O(x,s) = -\frac{i_F(s)\left[\exp(\lambda_1 x) + \exp(-\lambda_1 x)\right]}{zFD\lambda_1\left[\exp(\lambda_1\delta) - \exp(-\lambda_1\delta)\right]} \tag{18}$$

Considering $x=\delta$ and trigonometric identities in Eq. 18 yields:

$$c_O(\delta,s) = -\frac{i_F(s)\coth(\lambda_1\delta)}{zFD\lambda_1} \tag{19}$$

Eq. 19 can be represented in the frequency domain with $s = j\omega$

$$\tilde{c_O}(\delta, j\omega) = -\frac{\tilde{i_F}\coth(\lambda_1\delta)}{zFD\lambda_1} \tag{20}$$

where $j = \sqrt{-1}$ represents the imaginary component and ω represents the angular frequency.

The diffusion equation in the frequency domain (Eq. 20) can be represented as:

$$\tilde{\vartheta} = -\frac{\tilde{i_F}\coth(\lambda_1\delta)}{zFD\lambda_1 c_O^*} \tag{21}$$

where $\tilde{\vartheta} = \tilde{c_O}/c_O^*$ represents the oscillating ratio during AC perturbation between concentration of chemical species at the electrode surface and bulk concentration.

2.2 Electrochemical Impedance of NiMH Batteries

Substituting Eq. 21 into Eq. 7 yields:

$$\tilde{i}_F = \frac{1}{R_C}\tilde{V} - i_0 \exp\left(-\eta_{ss}/b\right)\left(\frac{\tilde{i}_F \coth\left(\lambda_1\delta\right)}{c_O^* zFD\lambda_1}\right) \tag{22}$$

Eq. 22 can be rearranged as:

$$\tilde{i}_F\left\{R_C + R_C i_0 \exp\left(-\eta_{ss}/b\right)\left(\frac{\coth\left(\lambda_1\delta\right)}{c_O^* zFD\lambda_1}\right)\right\} = \tilde{V} \tag{23}$$

Substituting *Rc*, which is represented through Eq. 8, into the second term on the left-hand side of Eq. 23 yields:

$$\tilde{i}_F\left(R_C - \frac{b\coth\left(\lambda_1\delta\right)}{zF\vartheta_{ss}c_O^* D\lambda_1}\right) = \tilde{V} \tag{24}$$

The use of a small AC perturbation superimposed into the V-I response of an electrochemical system allows the use of a linear model for system characterisation using EIS. Eq. 25 is an expression to relate Butler-Volmer Equation (Eq. 3) into a linear representation $i = -i_0 f\eta$ [28] of the V-I curve (see Appendix B).

$$\frac{RT}{zF} = -\frac{b}{\vartheta_{ss}} \tag{25}$$

Substituting Eq. 25 into Eq. 24 yields:

$$\tilde{i}_F\left(R_C + \frac{RT\coth\left(\lambda_1\delta\right)}{z^2F^2c_O^* D\lambda_1}\right) = \tilde{V} \tag{26}$$

Eq. 26 can be rearranged as:

$$\tilde{i}_F = \frac{\tilde{V}}{R_C + Z_W} \tag{27}$$

where:

$$Z_W = R_W \frac{\coth\left(j\omega T_W\right)^{0.5}}{\left(j\omega T_W\right)^{0.5}} \tag{28}$$

is known as the finite-space diffusion Warburg Impedance and represents the transition from Warburg behaviour (45◦ line) to a capacitive behaviour in the lower frequency range [35], with $\lambda_1 = \sqrt{j\omega / D}$

$$R_W = \frac{RT\delta}{z^2 F^2 c_O^* D} \tag{29}$$

defined as resistance for the diffusion process and

$$T_W = \frac{\delta^2}{D} \tag{30}$$

defined as the time constant for diffusion of chemical species.

The current due to double layer charge capacitance between dissimilar materials in the electrode is expressed as:

$$i_{C_{dl}} = C_{dl} \frac{dV}{dt} \tag{31}$$

where C_{dl} is the double layer capacitance between electrode and electrolyte. Applying the Taylor series expansion expressed in Eq. 5 into Eq. 31 yields:

$$\tilde{i}_{C_{dl}} = C_{dl}(j\omega)\tilde{V} \tag{32}$$

The electrochemical reaction in a battery results in an inhomogeneous distribution of charge in the electrode. As a result, a non-ideal capacitive behaviour has to be considered in the theoretical treatment. In order to correct for this inhomogeneity, a constant phase element (CPE) is used in Eq. 32 to replace the capacitor that represents the double layer capacitance C_{dl} [14,16].

$$\tilde{i}_{CPE} = Y_C (j\omega)^{P_C} \tilde{V} \tag{33}$$

when the value of P_C is equal 1, Eq. 33 becomes Eq. 32 to represent the current related to a pure capacitor.

The total current is defined as the sum between Faradaic current and charge capacitance current [22,36,37], as such:

$$\tilde{i} = \tilde{i}_F + \tilde{i}_{CPE} \tag{34}$$

Substituting Eqs. 27 and 33 into Eq. 34 gives:

$$\tilde{i} = \frac{\tilde{V}}{R_C + Z_W} + Y_C (j\omega)^{P_C} \tilde{V} \tag{35}$$

The impedance response of the positive electrode in a NiMH battery is defined as the ratio between the oscillating voltage, and the oscillating current $Z_C = \tilde{V}/\tilde{i}$, as such:

$$Z_C = \frac{R_C + Z_W}{(R_C + Z_W) Y_C (j\omega)^{P_C} + 1} \tag{36}$$

The analytical expression represented in Eq. 36 is analogous to the impedance response of the parallel combination (Warburg element in series with the resistor-CPE) Randles electrical circuit used for EIS analysis on NiMH batteries. The Warburg element Z_W represented in Eq. 28 has been derived from diffusion theory considering reflective boundary conditions [33,38].

3. Experimental Validation

A 9.6 V rechargeable battery pack NiMH AA 2500 mAh was used for the experimental tests. The battery pack consisted of 8 cells with a nominal voltage of 9.6 V. The NiMH battery pack was charged and discharged using a Voltz 6250 synchronous balance charger. EIS measurements were carried out in the NiMH battery pack using a Solartron 1280C Frequency Response Analyser (FRA). EIS measurements were carried out at open circuit voltage (OCV) and zero DC current to ensure steady state conditions [6,39,40,41]. The NiMH battery was initially fully charged and then it was discharged at a constant current of 3.3 A until a voltage of 9.18 Volts was measured. The load was disconnected and the battery pack was left at open circuit (equilibrium condition) for one hour. Thereafter potentiostatic EIS measurements were carried out at zero DC current and at frequencies from 20 kHz to 0.005 Hz. The AC signal perturbation applied was 10 mV. Once the EIS measurements were completed, the battery pack was again discharged down to 9 Volts. EIS measurements were again carried out at zero DC current after one hour of rest at open circuit. The same procedure was carried out for EIS measurements at OCV of 8.4, 8, and 7.48 Volts. The measurements carried out at OCV ensured consistency with Kramers-Kronig relations and ensured no drift in the SOC,

especially during low frequency EIS measurements [39]. K-K consistency is very important for the validity of EIS measurements in electrochemical systems [34,42].

Figure 2 shows that there is a correlation between the EIS and the decrease in the SOC of the NiMH battery. Fig. 2b shows that the real part of the EIS measurements where the imaginary component Z'' intercepts the real axis Z' increases during the discharge of the battery. This effect has been reported as an increase of solution resistance or ohmic resistance in the electrolyte which dries out during deterioration of voltage performance [13]. The increase in ohmic resistance can also be related to a reduction of hydrogen ions and water in the electrolyte during the discharge of the NiMH battery. The pseudo-straight EIS measurements with negative imaginary component Z'' at low frequencies, which is related to diffusion mechanisms [14], increases with decreasing the SOC of the battery, as shown in Fig. 2a. The pseudo-straight EIS measurements with negative imaginary component Z'' have been related to the diffusion process of ions which can be simulated with the Warburg component [14]. As the electrochemical mechanisms in the electrodes of batteries and fuel cells are represented in the negative imaginary part of the complex-impedance-plane, the pseudo-straight EIS measurements with positive imaginary component Z'' of the complex-impedance-plane at high frequencies as shown in Fig. 2a is related to the inductance of the measurement cables [43]. The reversible voltage for the reaction of the positive electrode is around 0.48 V [44] and for the negative electrode is -0.83 V. The total reversible voltage per individual cell for the discharge reaction is around 1.31 V. In future work the EIS response of each individual cell will be simultaneously measured using a multi-channel FRA [45] to study inhomogeneities and overpotentials of each cell during battery stack operation.

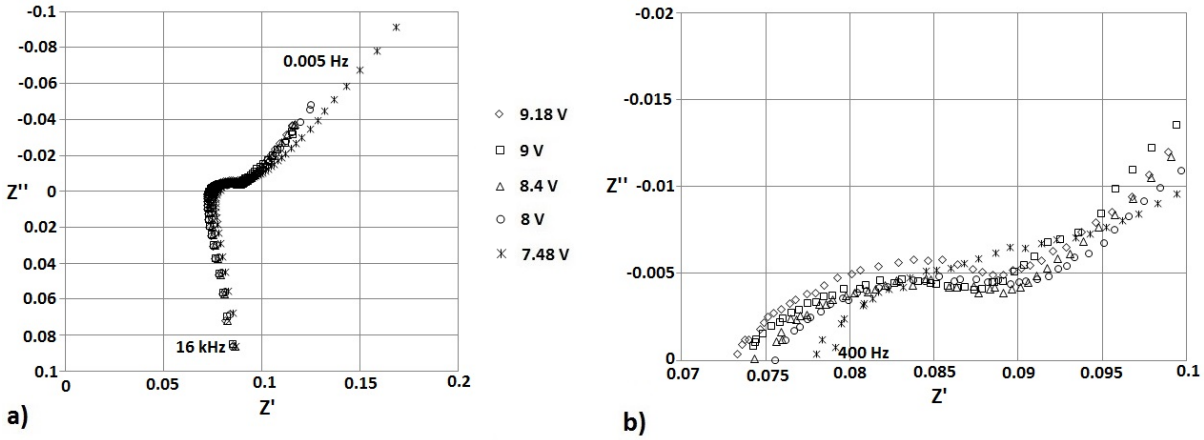

Figure 2. EIS measurements in NiMH Battery Pack, a) full spectra, b) high frequency region

The electrical circuit shown in Fig. 1 has been used to relate the EIS measurements at different SOC in NiMH batteries. In this study, the circuit shown in Fig. 1 and hence Eq. 36 will be applied to EIS measurements carried out in the NiMH battery pack. The electrical circuit shown in Fig. 1 was constructed and fitted to the EIS measurements using ZView software (Scribner Associates Inc.). ZView software is a tool to fit any electrical circuit with EIS data. The electrical components defined in ZView such as resistor, capacitor, inductor do not provide a direct relation within the electrochemical mechanisms. For instance, the Randles circuit constructed in ZView can represent the EIS resulting from an electron-transfer reaction between an electrode/electrolyte interface, but the resistor does not provide the direct relation with kinetics of the Redox reaction (Tafel slope, exchange current). Noting that the Warburg element corresponds to the type Open Circuit Terminus defined in ZView software. This type of Warburg element represents the transition from Warburg behaviour (45◦ line) to a capacitive behaviour in the lower frequency range due to the short diffusion lengths in the thin film in the electrode when the diffusion penetration depth can reach the reflective center of a nanoparticle at accessible low frequencies [22]. Nevertheless, the best fit was achieved by introducing a new time constant (resistor-CPE parallel configuration) in the circuit architecture shown in Fig. 1. This additional resistor-CPE (*Ra-CPEa*) parallel configuration as shown in Fig. 3 represents the electrochemical mechanisms in the negative electrode (anode) where hydrogen ions H^+ are released from the metal hydride alloy *MH*. The impedance response of the negative (MH) electrode can be derived from the Butler-Volmer equation and would result in a similar impedance equation as the one derived for the positive $Ni(OH)_2$ electrode, but neglecting diffusion mechanisms $Z_W=0$. Also, a resistor-inductor parallel configuration (R_L-L) was required to fit the EIS measurements with positive imaginary components Z'' related to the inductance of the measurement system. The inductance of the cables could be manifested as a straight-line perpendicular to the real axes Z'. In this case a single inductor L connected in series with the rest of the circuit will be sufficient to predict EIS measurements with positive imaginary components at high frequencies. Fig. 3 shows the electrical circuit constructed in ZView software for NiMH battery EIS analysis.

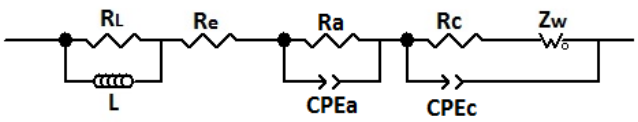

Figure 3. Electrical Circuit constructed in ZView for NiMH battery EIS analysis

The impedance of the circuit shown in Fig. 3 is expressed as:

$$Z = Z_L + R_e + \frac{R_a}{(R_a)Y_a(j\omega)^{P_a} + 1} + \frac{R_C + Z_W}{(R_C + Z_W)Y_C(j\omega)^{P_c} + 1} \tag{37}$$

with

$$Z_L = \frac{R_L L j\omega}{R_L + L j\omega}$$

where Z_L represents the impedance response of the inductance of the measurement cables, *Re* is the ohmic resistance in the electrolyte, the third term on the right hand side represents the impedance response for electrochemical mechanisms in the negative electrode (anode), and the fourth term represented in Eq. 36 is the impedance response for the electrochemical mechanisms in the positive electrode (cathode).

The circuit shown in Fig. 3 was fitted to the experimental measurements shown in Fig. 2 using ZView software. Fig. 4 shows that it is possible to reproduce the EIS measured using the electrical circuit shown in Fig. 3 (Eq. 37). The transition from Warburg behaviour (45◦ line) to a capacitive behaviour in the lower frequency range is masked in the simulated EIS data. Instead a CPE behaviour in the lower frequency range is observed, as shown in Fig. 4. It has been reported [22] that particle size distribution in battery electrodes may lead to a CPE behaviour [46] in the lower frequency range in the diffusion impedance of battery electrodes. The values of the electrical components resulted from fitting the circuit shown in Fig. 3 with EIS measurements are shown in Table 1. The least squares fitting method ensured the best fit between the model and the EIS data. A good quality fit is obtained when the sum of deviations squared between simulated and experimental data is at minimum (e.g. < 1).

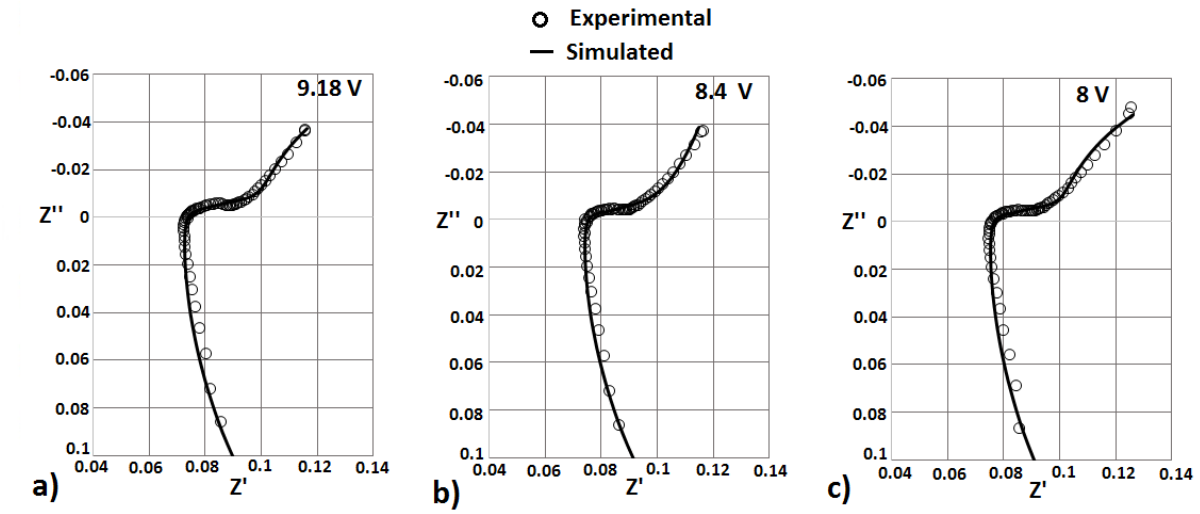

Figure 4. Comparison in Nyquist format between experimental and simulated data from Eq. 37, a) 9.18V, b) 8.4 V, c) 8 V

A comparison in Bode format between the model and experimental results as shown in Figs. 5 and 6 demonstrates that the model can predict the experimental measurements under the operating frequency tested. Orazem and Tribollet [47] reported that the Bode modulus and real part component of the impedance plots are relatively insensitive to the quality of the fit of a model to impedance data. The imaginary component of the impedance and Bode phase angle plots are modestly sensitive to fit quality.

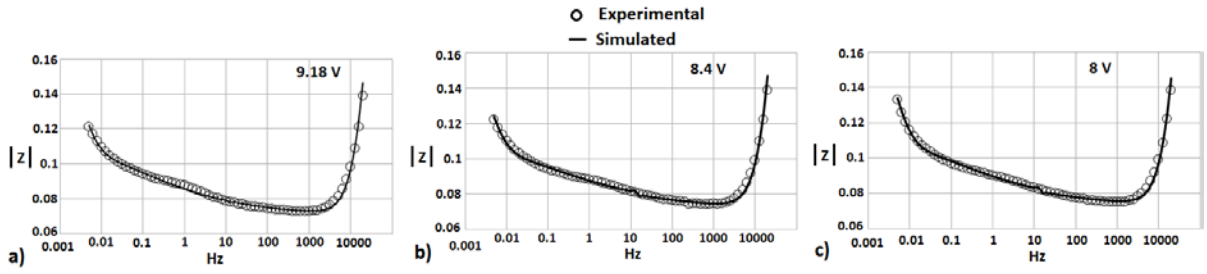

Figure 5. Comparison in Bode format (modulus) between experimental and simulated data from Eq. 37, a) 9.18V, b) 8.4 V, c) 8 V

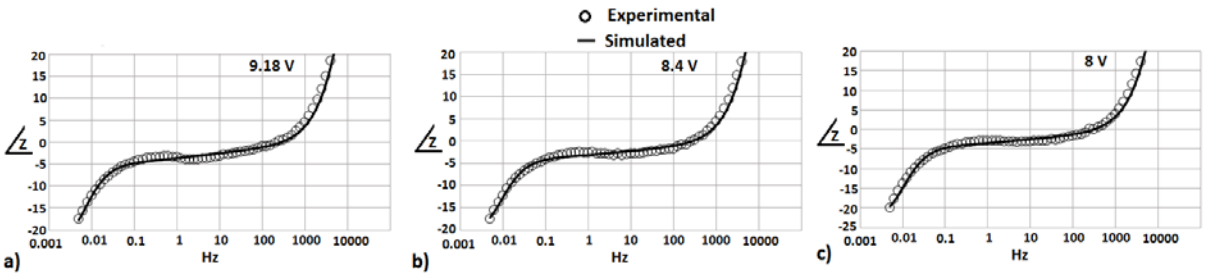

Figure 6. Comparison in Bode format (phase) between experimental and simulated data from Eq. 37, a) 9.18V, b) 8.4 V, c) 8 V

Table I. Values of electrical components resulted from fitting circuit shown in Fig. 3 with EIS measurements.

OCV	L H	R_e Ω	R_a Ω	Y_C $(sec)^P/\ \Omega$	P_C	R_C Ω	R_W Ω	T_W sec
9.18 V	9.3525E-7	0.070171	5.41E-7	28.71	0.27955	0.069913	0.00072545	0.179
9 V	9.2068E-7	0.070982	0.001453	35.9	0.2607	0.065775	0.00065346	0.1206
8.4 V	9.2765E-7	0.071799	0.00134	30.54	0.26772	0.058387	0.00027517	0.059493
8 V	9.1226E-7	0.072751	0.001212	27.14	0.28125	0.060897	0.00021685	0.039289
7.48 V	8.9168E-7	0.075805	0.000887	19.69	0.34881	0.10318	0.00015926	0.0074939

Table I demonstrates that the ohmic resistance R_e in the electrolyte increases during the discharge of the battery. This is consistent with the results reported by Cheng *et al.* [13]. The charge transfer resistance R_a in the anode for the oxidation of *MH* to release hydrogen ions H^+ is smaller (one order of magnitude) than the charge transfer resistance R_C in the cathode for the reduction mechanisms taking place in the positive electrode. Therefore, the limiting process is the reduction mechanism in the positive electrode $NiOOH + H_2O + e^- \rightarrow Ni(OH)_2 + OH^-$. The charge transfer resistance in the positive electrode R_C decreases with decreasing the SOC. This can be attributed to an increase in the driving force for the interfacial reduction process. The resistance for the diffusion process R_W decreases when the battery is discharged. The time constant T_W for the diffusion process decreases with decreasing the SOC in the battery as well. R_W and T_W are represented through Eqs. 29 and 30 respectively and are a function of the finite diffusive distance δ. A decrease in the diffusive distance decreases the values of R_W and T_W. The effect of R_W and T_W on EIS measurements will be discussed in the next section. During the discharge of the battery the amount of electroactive material for chemical species to diffuse is consumed and it cannot be replaced.

4. Effect of diffusion parameters on EIS measurements

Diffusion parameters have an effect on EIS measurements at low frequencies. The simulated EIS spectrum shown in Fig. 4 was taken as a reference to simulate the effect of R_W and T_W on EIS measurements. The simulated spectrum taken as a reference considers the parameters shown in Table 1 when the battery is discharged at 8.4 Volts. The resistance for the diffusion process R_W was increased and reduced by 70 % as shown in Fig. 7. The magnitude of the pseudo-straight EIS measurements at low frequencies increases with increasing R_W and decreases with decreasing R_W by 70%, as shown in Fig. 7. On the other hand, the magnitude of the pseudo-straight EIS measurements at low frequencies increases with decreasing T_W and decreases with increasing T_W by 70%. From Table 1, R_W decreased by 88% from high SOC at 9.18 Volts to the low SOC condition at 7.48 Volts. T_W decreased by 96 % from high SOC at 9.18 Volts to the low SOC condition at 7.48 Volts. The increase in magnitude of the pseudo-straight EIS measurements at low frequencies during the discharge of the battery shown in Fig. 2 is mainly attributed to a reduction of T_W. T_W and R_W are a function of the diffusive distance δ for chemical species to diffuse.

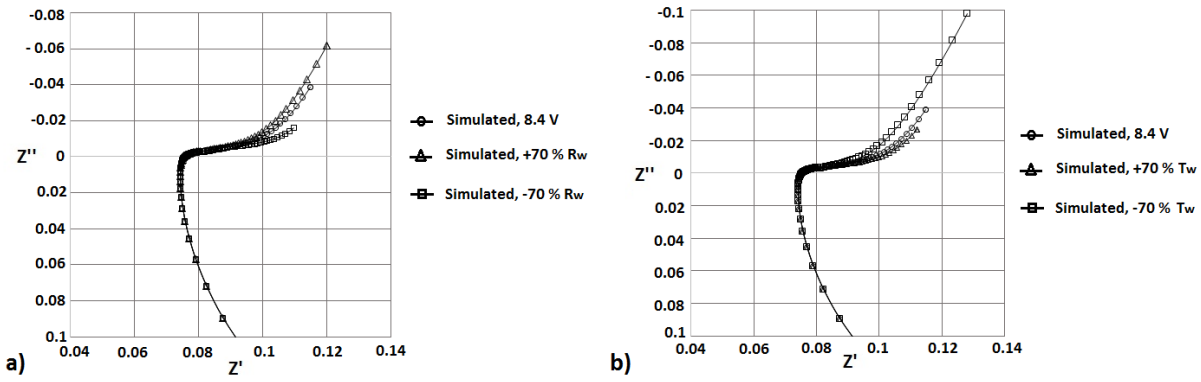

Figure 7. Effect of diffusion parameters on EIS spectrum, a) increasing/decreasing R_W, b) increasing/decreasing T_W

5. Discussion

During battery discharge H^+ ions released from the *MH* alloy structure in the negative electrode (anode) react with hydroxide ions OH^- from the electrolyte to produce H_20. Water in the electrolyte is dissociated into ions H^+ and OH^- respectively. Ions H^+ released from water in the electrolyte are absorbed into the positive electrode to form $Ni(OH)_2$. *D.* Zhu *et al*. [14] reported that the diffusion process of protons in the positive electrode (cathode) is

considered as the rate-limiting process under normal discharge which can be simulated through the Warburg component. A decrease in the diffusive distance δ during the discharge of the battery decreases the diffusion time constant T_W. As the reaction rate of ions to form nickel hydroxide becomes faster during the discharge of the battery, therefore the diffusive time constant for ions to be adsorbed in the cathode decreases. It has been reported, an intermediate reaction to release ion and hydroxide ion from water in the reaction that forms $Ni(OH)_2$ [14,27]. Based on these EIS results it is possible to speculate that initially during the discharge of the NiMH battery at high SOC, ions released from water near the negative electrode will diffuse through the electrolyte to reach the positive electrode and form $Ni(OH)_2$. As the reaction rate of $Ni(OH)_2$ and consumption of ions increases during the discharge of the NiMH battery, ions available near the positive electrode will diffuse and adsorb into the cathode. This effect would decrease the diffusion distance δ in R_W and T_W expressed in Eqs. 29 and 30 for ions to reach the positive electrode and hence react with $NiOOH$ to produce $Ni(OH)_2$. As the SOC decreases in the battery, the concentration of available ions for the $Ni(OH)_2$ production in the positive electrode would severely decrease. This effect could justify the increase in charge transfer resistance R_C expressed in Table I for EIS measurements with lower SOC (7.48V). R_C is a function of concentration of chemical species ϑ_{ss} as shown in Eq. 8. EIS measurements carried out at in NiMH at the lowest SOC will be modelled and studied considering overdischarge reaction [24]. This is the aim of future work. The low frequency EIS measurements of individual batteries have been commonly modelled with a Warburg element which represents a semi-infinite linear diffusion and can be represented with a line with a slope of 1 (or 45° with respect to the real axis) in the low-frequency part of the Nyquist plot. As shown in Fig. 4, the slope of the pseudo-straight line at low frequencies is not 45° with respect to the real axis Z'. As demonstrated, the EIS results at low frequencies can be predicted by a Warburg element derived from diffusion theory considering reflective boundary conditions. The diffusive time constant *Tw* for the Warburg element (Open Circuit Terminus) defined in ZView software relates the transition from Warburg behaviour (45◦ line) to a capacitive behaviour in the lower frequency range due to the short diffusion distance to reach the reflective center of a nanoparticle at accessible low frequencies [22]. Also, the change in the slope of the pseudo-straight line (CPE behaviour) at low frequencies can be related to the effect of actual particle geometry and size distribution of an electrode on Impedance measurements. Particle

geometry as well as size distribution will be considered in a future modelling work to accurately interpret impedance spectra of battery electrodes.

6. Conclusion

In this study, an impedance model for EIS analysis during the discharge of a NiMH battery has been developed. Electrochemical and diffusion theories were considered for the development of the mathematical treatment. The analytical model is analogous to the impedance response of the Randless Circuit commonly used for NiMH battery characterisation using EIS. The model was validated against EIS measurements carried out in a NiMH a different SOC using ZView software. The impedance model can predict the EIS response and can provide an insight into the electrochemical mechanisms involved during the discharge of the NiMH battery. The results showed that the model has established a backbone understanding of how the electrochemical mechanisms relate to the electrochemical impedance spectra of the NiMH battery. In future work overdischarge reaction at abnormal severe operating conditions will be considered to study SOH in NiMH batteries.

Appendix A.

Solution of Fick´s Second Law in the Laplace domain.

$$D\frac{\partial^2 c_O(x,t)}{\partial x^2} = \frac{\partial c_O(x,t)}{\partial t} \tag{A.1}$$

Transforming Eq. A.1 in the Laplace domain and considering the initial condition at *t=0* as $c_O(x,0) = 0$ gives:

$$D\frac{\partial^2 c_O(x,s)}{\partial x^2} = sc_O(x,s) \tag{A.2}$$

Eq. A.2 can take the form of a homogenous equation:

$$a\frac{\partial^2 \lambda}{\partial x^2} + b\frac{\partial \lambda}{\partial x} + c\lambda = 0 \tag{A.3}$$

which has the following roots:

$$\lambda_{1,2} = \pm\sqrt{s/D} \tag{A.4}$$

The solution of a homogeneous equation with different roots can be obtained as follows:

$$c_O(x,s) = A\exp(\lambda_1 x) + B\exp(\lambda_2 x) \tag{A.5}$$

Appendix B.

The Butler-Volmer Equation considering oxidation/reduction processes:

$$\frac{i}{i_0} = \frac{c_O}{c_O^*}\exp(-\alpha f\eta) - \frac{c_R}{c_R^*}\exp((1-\alpha)f\eta) \tag{B.1}$$

With $f = zF/RT$

A Linear representation with Taylor series expansion [28] is expressed as:

$$\frac{i}{i_0} = \frac{c_O}{c_O^*} - \frac{c_R}{c_R^*} - \frac{zF}{RT}\eta \tag{B.2}$$

An expression to relate Butler-Volmer Equation (Eq. B.1) into a linear representation $i = -i_0 f\eta$ [28] of the V-I curve can be defined as:

$$\frac{RT}{zF} = -\frac{b}{\vartheta_{O,R}} \tag{B.3}$$

Substituting Eq. B.3 into Eq. B.2 yields:

$$\frac{i}{i_0} = \frac{c_O}{c_O^*} - \frac{c_R}{c_R^*} + \frac{\vartheta_{O,R}\eta}{b} \tag{B.4}$$

where $\vartheta_{O,R} = \frac{c_{O,R}}{c_{O,R}^*}$ is the ratio between chemical species at electrode surface and bulk concentration.

Eq. B4 can be rearranged as:

$$\eta = \frac{b}{\vartheta_{0,R}} \frac{i}{i_0} + \frac{b}{\vartheta_R} \frac{c_R}{c_R^*} - \frac{b}{\vartheta_O} \frac{c_O}{c_O^*} \tag{B.5}$$

Eq. B.5 can be expressed as:

$$\frac{b}{\vartheta_{O,R}} \frac{i}{i_0} = \eta \tag{B.6}$$

Substituting Eq. B.3 into Eq. B6 yields:

$$i = -i_0 f \eta \tag{B.7}$$

Eq. B7 represents the linear characteristics of the V-I curve.

List of Symbols

b	tafel slope (V)
c_O	surface concentration of oxygen (mol/cm^3)
c_O, c_R	surface concentration of species (mol/cm^3)
c_O^*, c_R^*	concentration of species in equilibrium (mol/cm^3)
C_{dl}	capacitance between dissimilar materials (F/cm^2)
D	effective diffusion coefficient (cm^2/s)
E^O	potential in electrode at equilibrium (V)
F	faraday constant (96485 C/mol)
f	frequency (Hz)
i	current density (A/cm^2)
i_o	exchange current density (A/cm^2)
$\tilde{i}$	deviation of variable i in the steady-state i_{ss}. (A/cm^2)
j	imaginary component in impedance
L	inductance of measurement cables, (H)
P	parameter related to CPE (dimensionless)
R	ideal gas constant (8.3143 J/mol-K)
R_a	charge transfer resistance in anode (Ω.cm^2)
R_C	charge transfer resistance in cathode (Ω.cm^2)

R_e	ohmic resistance in electrolyte ($\Omega.cm^2$)
R_W	resistance for the diffusion process ($\Omega.cm^2$)
T	temperature (K)
T_W	time constant for the diffusion process (s)
t	time, (s)
V	battery voltage (V)
$\tilde{V}$	deviation of variable V in the steady-state V_{ss}. (V)
v	flux of chemical species (mol/cm^2s)
x	distance along the diffusive distance $(0 \le x \le \delta)$
Y	parameter related to CPE ($s^P/\Omega.cm^2$)
Z	impedance of battery ($\Omega.cm^2$)
Z_C	impedance of cathode ($\Omega.cm^2$)
Z_W	Warburg impedance ($\Omega.cm^2$)
z	electrons released or consumed
Z'	real part of impedance ($\Omega.cm^2$)
Z''	imaginary part of impedance ($\Omega.cm^2$)

Greek

α	charge transfer coefficient
δ	diffusive distance (cm)
η	overpotential (V)
η_{SS}	overpotential in steady-state (V)
ω	angular frequency (rad/s)
ϑ	ratio between chemical species at the electrode surface and bulk concentration of chemical species, dimensionless
$\tilde{\vartheta}$	oscillating ratio during AC perturbation between concentration of chemical species at the electrode surface and bulk concentration, dimensionless.

References

[1] R. S. Robinson, *in Proceedings of Intelec'96-International Telecommunications and Energy Conference*, PV 22-6, p. 654, Massachusetts USA (1996).
[2] G. Alber and M. W. Migliaro, *in Proceedings of Intelec'94-International Telecommunications and Energy Conference*, PV10-1, p. 245, Vancouver B.C., Canada, (1994),
[3] J. D. Kozlowski, C. S. Byington, A. K. Garga, M. J. Watson, T. A. Hay, *in 2001 IEEE Aerospace Conference Proceedings*, PV 6, p. 3149, Montana, (2001).
[4] Y. K. Muramatsu; *Battery condition monitor and monitoring method*, United State Patent; 4,678,998; (1987)
[5] F. Huet., *J. Power Sources*, **70**, 59 (1998).
[6] K. Bundy, M. Karlsson, G. Lindbergh, A. Lundqvist, *J. Power Sources*, **72**, 118, (1998).
[7] S. Rodrigues, N. Munichandraiah, A.K. Shukla, *J. Solid State Electrochem*., **3**, 397, (1999).
[8] R. Minganta, J. Bernarda, V. S. Moynot, A. Delaille, S. Mailley, J-L. Hognon, F. Huet, ECS Trans., 33(39) 41, (2011).
[9] W. Haiying, H. Long, S. Jianhua, L. Shuanquan, W. Feng, *in Proceedings of 6th International Forum on Strategic Technology*, p. 261, Harbin China (2011).
[10] S. R. Nelatury, P. Singh, *J. Power Sources*, **132**, 309, (2004).
[11] M. L. Gopikanth, S. J. Sathyanarayana, J. Appl. Electrochem., **9**, 369, (1979).
[12] D. A. Howey, P. D. Mitcheson, V. Yufit, G. J. Offer, N. P. Brandon, *IEEE Trans. Veh. Technol.*, **63**, 2557, (2014).
[13] S. Cheng, J. Zhang, M. Zhao, C. Cao, *J. Alloys Compd*, 293–295, 814, (1999).
[14] Y. Zhu, W. H. Zhu, Z. Davis, B. J. Tatarchuk, *Adv. Phys. Chem*., 2016, ID 4584781, 11 pages, (2016).
[15] K. Onda, M. Nakayama, K. Fukuda, K. Wakahara, T. Araki, *J. Electrochem. Soc*., **153**, A1012, (2006).
[16] C. H. Hsu, F. Mansfeld, *Corrosion*, **57**, 747, (2001).
[17] C. Criado, P. Galán-Montenegro, P. Velásquez, J.R. Ramos-Barrado, *J. Electroanal. Chem*., **488**, 59, (2000).
[18] F. Sholz, Electroanalytical Methods, Springer, Heidelberg, (2010).
[19] M. Thele, M. Radin-Macukat, D. U. Sauer, O. Bohlen, D. Linzen, *in The 22nd International Battery, Hybrid and Fuel Cell Electric Vehicle Symposium & Exposition*, p. 1364, Yokohama, Japan (2006).
[20] S. Buller, M. Thele, E. Karden, R. W. De Doncker, *J. Power Sources*, **113**, 422, (2003).
[21] E. Kuhn, C. Forgez, P. Lagonotte, and G. Friedrich, *J. Power Sources*, **158**, 1490, (2006).
[22] J. Song, M. Z. Bazant, *J. Electrochem. Soc*. **160**, A15, (2013).
[23] J. J. C. Kopera, *Inside the Nickel Metal Hydride Battery*, p. 5 Texaco Ovonic Battery System LLC, (2002).
[24] R-S. Liu, L. Zhang, X. Sun, H. Liu, and J. Zhang, Electrochemical Technologies for Energy Storage and Conversion, Vol.1, Wiley-VCH, Weinheim, (2012).
[25] A. Forrest, *Modern Battery Technology*, Trumbore ed., Center for Professional Advancement, (1995).
[26] S. Rodrigues, N. Munichandraiah, A.K. Shukla, *J. Power Sources*, **87**, 12, (2000).
[27] A. H. Zimmerman and P. K. Effa, J. *Electrochem. Soc*., 131, 709, (1984).
[28] A. J. Ballard, and L. R. Faulkner, Electrochemical Methods, John Wiley & Sons, New York, (2001).
[29] W.B. Gu, C.Y. Wang, S.M. Li, M.M. Geng, B.Y. Liaw, Electrochim. Acta, **44,** 4525, (1999).
[30] O. Barbarisi, R. Canaletti, L. Glielmo, M. Gosso, F. Vasca, *In Proceedings of the 41st IEEE Conference on Decision and Control*, p.1739, Las Vegas, USA, (2002).
[31] S. Raël, M. Hinaje, *J. Power Sources*, 222, 112, (2013).
[32] N. A. Chaturvedi, R. Klein, J. Christensen, J. Ahmed, A. Kojic, *IEE Control Syst. Mag*., **30**, 49 (2010).
[33] J. Bisquert, G. Garcia-Belmonte, F. Fabregat-Santiago, P. R. Bueno, *J. Electroanal. Chem*, **475**, 152, (1999).
[34] S. Cruz-Manzo, R. Chen, P. Greenwood, *Insights Anal. Electrochem*., 1:1 (2015).
[35] M. D. Levi, D. Aurbach, *J. Phys. Chem. B*, **101**, 4630, (1997).
[36] J. E. B. Randles, *Discuss. Faraday Soc*, **1**, 11, (1947).
[37] D. C. Grahame, *J. Electrochem. Soc*, **99**, 370C, (1952).
[38] R. Macdonald, Impedance Spectroscopy, Wiley Interscience, New York, (1987).
[39] A. Hammouche, E. Karden, R. W. D. Doncker, J. Power Sources, **127**, 105, (2004).
[40] V. V. Viswanathan, A.J. Salkind, J. J. Kelley, J.B. Ockerman, *J. Appl. Electrochem*., **25,** 716, (1995).
[41] V. V. Viswanathan, A. J. Salkind, J. J. Kelley, J. B. Ockerman, *J. Appl. Electrochem*., **25**, 729, (1995).
[42] M. Urquidi-Macdonald, and S. Real, and D. D. Macdonald, *J. Electrochem. Soc*., **133**, 2018, (1986).
[43] S. Cruz-Manzo, R. Chen and P. Rama, *J. Fuel Cell Science Technology*, **9**, 051002, (2012).
[44] S. A. Hackney, R. V. Kumar, High Energy Density Lithium Batteries, Ed. K. E. Aifantis, Wiley-VCH, Weinheim, (2010).

[45] S. Cruz-Manzo, R. Chen, *J. Electrochem. Soc*., **160**, F1109, (2013).
[46] J. Bisquert, G. Garcia-Belmonte, P. Bueno, E. Longo, L.O.S. Bulhões, *J. Electroanal. Chem*., **452**, 229, (1998).
[47] M. Orazem, B. Tribollet, Electrochemical Impedance Spectroscopy, Wiley, New Jersey, 2008.